Journal of Molecular Spectroscopy 386 (2022) 111603

Contents lists available at ScienceDirect

Journal of Molecular Spectroscopy

journal homepage: www.elsevier.com/locate/yjmsp

The atmospheric continuum in the "terahertz gap" region (15–700 cm^{-1}): Review of experiments at SOLEIL synchrotron and modeling

T.A. Odintsova [a,*], A.O. Koroleva [a,b], A.A. Simonova [c], A. Campargue [b], M.Yu. Tretyakov [a]

[a] Institute of Applied Physics of RAS, Nizhniy Novgorod, Russia
[b] Univ. Grenoble Alpes, CNRS, LIPhy, Grenoble, France
[c] V.E. Zuev Institute of Atmospheric Optics SB RAS, Tomsk, Russia

ARTICLE INFO

Keywords:
SOLEIL synchrotron
Atmospheric continuum
THz gap
Dimer
Far wings

ABSTRACT

The results of our recent water vapor related continuum studies in the range of the "terahertz gap" at the AILES beam line of the SOLEIL synchrotron using a Fourier transform spectrometer are reviewed and summarized. The continuum of pure water vapor and its mixture with N_2, O_2 and dry air were investigated in the 15–700 cm^{-1} range in conditions close to the atmospheric ones. Analysis of the frequency and temperature dependence of the self-continuum revealed a significant contribution of a stable water dimer to the observed absorption, which is not taken into account by the MT_CKD semi-empirical model of the continuum widely used for atmospheric applications. We propose a physically based approach to continuum modeling, which explicitly accounts for the contribution of dimers and far wings of monomer resonance lines. We applied the suggested approach for the water vapor self-continuum modeling in the H_2O rotational band and supported it by comparing with the SOLEIL data. The frequency dependence of the relative contributions of far wings, stable and metastable dimers to the self-continuum is evaluated. Prospects for further developments of the atmospheric continuum modeling are considered.

1. Introduction

Despite the recent progress, the terahertz frequency range (0.3–10 THz or 10–300 cm^{-1}) remains poorly studied, mostly due to the lack of available radiation sources and receivers. For this reason and due to its location between the microwave and infrared ranges, it is called the "terahertz gap" (see the reviews [1,2] and references therein). The THz gap is interesting because it contains absorption spectra of many astrophysical, organic and atmospheric molecules. For example, significant lines of the pure rotational absorption spectrum of water vapor extends to a frequency of about 18 THz (600 cm^{-1}), *i.e.* the main part of the band falls into the THz gap. In addition, the maximum of the outgoing heat flux of the Earth falls in the THz range. The development of high-speed wireless communication systems in the THz range requires allowance for atmospheric absorption, mainly due to water vapor. Also, to accurately model the Earth's radiation balance it is necessary to take into account the atmospheric absorption, in particular, water vapor absorption.

The absorption of electromagnetic radiation by water vapor – the main greenhouse gas in the Earth's atmosphere – is traditionally subdivided into two components, namely, the *resonance absorption* (the sum of the absorption lines, corresponding to roto-vibrational transitions of water monomers) and the *continuum absorption* smoothly varying with frequency, or just the continuum (absorption under the resonance lines). The resonance absorption has been much better characterized both theoretically and experimentally than the continuum. This is due to *(i)* the difficulty to measure accurately weak continuum absorption and *(ii)* the fact that the continuum is determined as a difference between experimental water vapor absorption and calculated resonance absorption spectrum and, therefore, strongly depends on the line shape model and on the accuracy of its parameters. Compared to the resonance absorption, the relative magnitude of the continuum varies strongly: the continuum can be several orders of magnitude weaker than the resonance absorption near the line center and by one order of magnitude (and even more) stronger in between H_2O lines (the so-called "atmospheric" microwindows). The water vapor continuum has to be accounted for in the radiative transfer codes modeling our atmosphere. Currently, a semi-empirical continuum model – the MT_CKD [3] – is widely used for atmospheric applications. Our recent experimental studies [4–7] have been motivated by the need to validate the MT_CKD continuum model in the THz range. In addition, these new data may give new insights into the physical origin of the continuum and serve as the

* Corresponding author.

https://doi.org/10.1016/j.jms.2022.111603
Received 3 December 2021; Received in revised form 3 March 2022; Accepted 4 March 2022
Available online 9 April 2022

basis for a physically based continuum modeling in a wide range of frequencies and thermodynamic conditions. It is well known that the continuum arises from the collisional interaction of molecules [8], in particular, mainly due to *pair interactions* because triple effects can be neglected at atmospheric conditions. Thus, the continuum magnitude varies as the product of interacting molecules concentrations (or partial pressures).

The atmospheric continuum consists of a dry and a wet component. The *dry continuum* arises mainly from the interaction of nitrogen and oxygen molecules. The *wet continuum* is related to atmospheric water vapor and arises from the interaction of water molecules with each other (*self-continuum*) and with other atmospheric molecules (*foreign-continuum*). Pair interaction of molecules leads to *(i)* the formation of bimolecular states including metastable (quasibound) and stable (truly bound) dimers and free-pair states (the latter is known to be a dominant contributor to the dry continuum [8–10] but provides negligible contribution to pure water vapor in usual atmospheric conditions [11–13]) and *(ii)* the deviation of the "observed" far wings of the molecular lines from the theoretical profiles derived in the impact approximation [14–16]. Each continuum component varies smoothly with frequency, which makes it difficult to disentangle the two contributions. Two complementary hypotheses on the continuum origin, based on the two aforementioned mechanisms, were suggested long ago. The hypothesis of the dominant role of far wings of water lines is supported by the fact that the sophisticated theoretical [17,18] and the semi-empirical [19] modifications of line profile at large detuning from the line center were able to empirically account for the scarce experimental data at disposal. This approach is the basis of the MT_CKD model [3]. However, as demonstrated in [20] and in the subsequent study [21], the spectral features observed in the continuum in the mm-submm wave range (0.1–0.26 THz or 3.5–8.7 cm^{-1}) can be unambiguously attributed to stable water dimer absorption. Moreover, quantitative evaluation of the dimer absorption led to the conclusion that this mechanism is dominant in water vapor continuum in this spectral range. Evidence of stable water dimer absorption within H_2O fundamental vibrational bands was also demonstrated [22,23]. It should be mentioned that different continuum constituents are expected to have different temperature dependence [11] which could help to discriminate them. These facts form the general theoretical ground for the analysis of the continuum composition.

The THz range is very attractive for studying the continuum, mainly because the results of global sophisticated *ab initio* calculations of the bound water dimer spectrum are available in this region [24]. All possible rotational-vibrational tunneling transitions of the dimer up to its first dissociation limit are explicitly taken into account in these calculations, contrary to the simplified calculations in the IR range (see *e.g.* [25,26] and refs therein), which consider the dimer as two individually vibrating monomer units and neglect the low frequency modes involving both molecules (only band centers and band intensities are calculated). The detailed knowledge of the dimer spectrum in the THz range is expected to help to evaluate other physical mechanisms contributing to the measured continuum.

For quantitative spectroscopic studies of the continuum absorption in the THz range, a powerful radiation source operating in a broad frequency range is needed. Keeping in mind the characteristic scale of the continuum variation with frequency (hundreds of GHz), the desired operating range of the source should cover tens of THz. The high power, large spectral coverage and high stability of the SOLEIL synchrotron make it an ideal source for this kind of studies.

Since 2014, several experimental campaigns have been organized (SOLEIL Projects Nos. 20140227, 20170067 and 20180347), aiming at studying the water vapor continuum in the frequency range of a pure rotational water band (about 0.45–21 THz or 15–700 cm^{-1}). The results of the analysis of the recorded spectra together with the obtained continuum cross-sections have been reported in a series of papers [4–7]. The present contribution summarizes the conclusions of these investigations. Furthermore, the approach for physically based continuum modeling is outlined and is applied to the SOLEIL measurements of the self-continuum in the pure rotational water band. This allows making quite definite conclusions about bimolecular absorption and far wings contributions.

For the reader's convenience, we briefly recall in the next section the main characteristics of the measurement method and the experimental conditions and summarize the obtained experimental data. In the third section, we propose a physically based absorption model, which includes the continuum in a natural way, and demonstrate the application of its simplified version to the THz region. In the Conclusion, the main results of the trial and prospects for further developments are presented.

2. Experimental data

2.1. FTS recordings

Spectra were recorded at the AILES beamline of SOLEIL synchrotron using a high–resolution Fourier-Transform spectrometer (Bruker IFS–125HR). Coherent radiation (CR) and standard radiation (SR) synchrotron operation modes were used to cover the 15–35 cm^{-1} and 40–700 cm^{-1} spectral intervals, respectively. The summary of the various experimental conditions of the recordings is presented in Table 1. A multiple reflection cell with effective path length of 151.75 m was used. To record spectra at elevated temperature (326 K), the cell was wrapped with several 60 °C silicon rubber heaters and additional thermal isolation. To evaluate and exclude possible bias due to a change of the base line related to the pressure variation, a two-step procedure was adopted for the gas mixture. At the first step, the cell was filled with pure water vapor, and then a foreign gas was gradually added. At the second step, the resulting mixture was gradually pumped out. Note that for the 16 mbar maximum water pressure value used for the recordings (Table 1) the relative humidity did not exceed 60%. It was assumed that the water vapor pressure is constant during filling and decreases in proportion to the total mixture pressure during pumping out. This was generally confirmed by the retrieval of the water concentration from a line shape fitting of unsaturated water lines. It should be mentioned that effects of adsorption–desorption of water in the cell were not evidenced during the experimental studies (for instance, water vapor pressure was observed to stabilize almost instantaneously after the injection). Such effects are negligible because of the very large volume of the used gas cell compared to its inner surface area.

2.2. Analysis and cross-section retrieval

The experimental transmittance, Tr, is related to the absorption coefficient, α, by $Tr = \exp(-\alpha L) \otimes f_{app}$, where L and f_{app} are the absorption pathlength and the apparatus spectral resolution function, respectively. The FTS spectra were analyzed using the commonly accepted approach: the difference between the measured (α) and the calculated resonance (α_R) absorption coefficients is referred to the continuum (α_C):

$$\alpha_C(\nu, T, P) = \alpha(\nu, T, P) - \alpha_R(\nu, T, P), \quad (1)$$

where ν, P and T are frequency, pressure and temperature, respectively. Resonance absorption was modeled as a line-by-line sum using the HITRAN line list for 6 most abundant water isotopologues [27] and Van Vleck–Huber line profile [28,19]. The standard far-wing cut-off at 25 cm^{-1} from the line center was applied, the far wings of the line below and above the cut-off frequency being excluded and the remaining almost rectangular absorption (the "pedestal" or "plinth") underneath the modeled line profile being preserved as an intrinsic part of the resonance absorption. Note that a different choice is made in the MT_CKD model for which the plinth is considered as part of the continuum. It should be mentioned that in the sub-THz frequency range (15 – 35 cm^{-1}), line shape parameters measured by microwave methods

Table 1
Experimental conditions of various recordings and the corresponding reference of their analysis.

Sample	Frequency range, cm^{-1}	Water pressure, mbar	Total pressure mbar	T,K	Resolution, cm^{-1}	Number of spectra	Ref.
$H_2^{16}O$	15–35	11–16	11–16	296	0.02	2	[4,5]
$H_2^{18}O$	15–35	13–16	13–16	296	0.02	2	[5]
$H_2^{16}O$	40–700	3–16	3–16	296, 326	0.02, 0.002	25	[4–6]
$H_2^{18}O$	50–500	2–6	2–6	296	0.02, 0.002	10	[5]
$H_2^{16}O$ – air	50–500	4	200–400	296	0.02	9	[7]
$H_2^{16}O$ – N_2	50–500	2–4	20–430	296	0.02	9	[7]
$H_2^{16}O$ – O_2	50–500	4	200–400	296	0.02	9	[7]

[29–34] were used instead of HITRAN values, when available. This allows us to determine the continuum practically in the whole spectral range recorded contrary to the majority of previous investigations in this range [35,36] and in the IR [36–38,22], where it was determined only at the points corresponding to microwindows of transparency due to the need to minimize the contribution of line parameter uncertainties.

The continuum absorption coefficient can be written as the sum of the self- (α_{self}) and foreign- (α_{for}) continua:

$$\begin{aligned}\alpha_C(\nu,T,P) &= \alpha_{self}(\nu,T,P)+\alpha_{for}(\nu,T,P)\\ &= C_s(T)P^2_{H_2O}/k_BT + C_f(T)P_{H_2O}P_{for}/k_BT\end{aligned} \quad (2)$$

Here, $C_s(T)$ and $C_f(T)$ are the self- and foreign-continuum cross-sections (in $cm^2molec^{-1}atm^{-1}$), k_B is Boltzmann constant, P_{H_2O} and P_{for} are water vapor and foreign gas partial pressure, respectively. For pure water vapor, only the first term of Eq. (2) remains.

The baseline stability of the spectra and the expected pressure dependences of the continuum absorption Eq. (2) were systematically checked confirming the reliability of the measurements: the continuum of pure water vapor increased quadratically with pressure (see *e.g.* Fig. 1 of [6]); the continuum of a mixture of water vapor with foreign gas increased linearly with the partial pressure of the added foreign gas (Fig. 2 of [7]) and decreased as the square of the total pressure during the pumping out of the mixture (Fig. 4 of [7]). In the 40–700 cm^{-1} spectral interval $C_s(T)$ and $C_f(T)$ values were found from a fit of the pressure dependence obtained at about 200 spectral points located in microwindows of transparency. Let us note that, although less accurate, the C_s values retrieved from wet gas mixtures are consistent with the values obtained with pure water vapor [7]. The $C_f(T)$ values obtained from the analysis of the data corresponding to filling and pumping stages are also in a good agreement.

The air-continuum cross-section of atmospheric water vapor, $C_{f\text{-}air}$, was obtained in two ways. In the first one, $C_{f\text{-}air}$ was retrieved directly from the experimental spectra of a mixture of water vapor with dry atmospheric air (see [7]). In the second case, $C_{f\text{-}air}$ was calculated from the $C_{f\text{-}N2}$ and $C_{f\text{-}O2}$ values retrieved from the spectra of water vapor with N_2 and O_2. Considering the dominant role of pair interactions and atmospheric abundances of major atmospheric gases N_2 (≈ 78%), O_2 (≈21%) and Ar (≈1%), $C_{f\text{-}air}$ can be expressed as:

$$C_{f-air} = 0.78C_{f-N2} + 0.21C_{f-O2} + 0.01C_{f-Ar} \quad (4)$$

Since the contributions of $C_{f\text{-}O2}$ and $C_{f\text{-}Ar}$ were found to be negligible [7,39], $C_{f\text{-}air}$ reduces to:

$$C_{f-air} = 0.78C_{f-N2} \quad (5)$$

The result agrees with the foreign-continuum retrieved from a mixture of H_2O with dry air [7]. Both, consistency of all experimental data sets with each other and expected pressure dependences serve as a tough validation of the obtained experimental data.

Temperature dependence of continuum cross-section $C(T)$ is empirically approximated using power law [40–42]:

$$C_{sf}(T) = C_{sf}(T_0)\cdot(T_0/T)^n, \quad (6)$$

where $T_0 = 296$ K, and n is the temperature exponent. The temperature exponent n of the self-continuum was estimated from C_s at 296 K and 326 K [6]. Since the temperature difference of the SOLEIL recordings was limited to 30 K, the above empirical law with one adjustable parameter was chosen instead of more complex functions (see, for example, [43,44]).

Fig. 1 presents an overview comparison of the water vapor self- and foreign-continua measurements available in the literature to our data and to the MT_CKD-3.2 model at 296 K. Note that SOLEIL C_s values with estimated uncertainty higher than 15% are not shown in Fig. 1, except in the low-frequency wing of the band (15–100 cm^{-1}), for which all available values are given (even with uncertainty higher than 50%). SOLEIL data and their uncertainties are given in Supplementary Materials of our previous papers [5–7]. Note that the estimated experimental uncertainty is often smaller that the spread of points observed in Fig. 1. The continuum is expected to vary smoothly with frequency and the observed dispersion reflects the uncertainty on the retrieved cross-sections, in particular, that related to the uncertainty of resonance line parameters. Overall, the SOLEIL results on self-continuum from [4–6] and the previous data [35,36,40,41,42,45,46,47] cover the whole range of the H_2O pure rotational band (significant lines of the band spread from 0.7 up to about 600 cm^{-1}). Note that the continuum around the intensity maximum of the H_2O rotational band (which is located around 150 cm^{-1} and coincides with the intensity maximum of the continuum) – from 84 to 350 cm^{-1} – has not been investigated before. Overall, using a wide variety of experimental conditions (pressure range, gas sample temperature, bolometer filter, synchrotron mode), our successive measurement campaigns at SOLEIL synchrotron allowed us collecting data covering the broad frequency range from 15 up to 700 cm^{-1} (with minor problems at the edges of the studied frequency range related to insufficient radiation power) and estimating the temperature dependence of the self-continuum in the 84 – 414 cm^{-1} region [6]. Data of different campaigns are consistent with each other. Above 350 cm^{-1} an excellent agreement with Burch's measurement is noted [36,37]. In the 3.5– 84.1 cm^{-1} low-frequency range, several studies are available [35,36,40–42,45–49]. Our C_s values in the 15 – 35 cm^{-1} range agree with the results of [35,36]. It is worth mentioning the encouraging agreement with unpublished results obtained by R. A. Bohlander and reported by Burch in 1981 [36]. Our comparison does not cover the results reported by [48,49] in the 10–33 cm^{-1} range because these broadband experimental data were fitted assuming a purely quadratic frequency dependence of the continuum absorption, thus only the mean values of $C_s(\nu)$ and $C_f(\nu)$ were determined throughout the studied range. Some deviations of our self-continuum from the literature data are observed in the range of 50.3–84.1 cm^{-1}, where our $C_s(\nu)$ values are smaller than the values reported in [45,46,36,35] by a factor between 1.5 and 2, respectively. These deviations can be explained by the measurements uncertainties: SOLEIL values were obtained from low signal-to-noise ratio spectra at the edge of the working range of the SR synchrotron mode, and the data by Podobedov [35] and Bohlander [36] show a large dispersion reflecting their uncertainties.

For proper comparison of our data with the MT_CKD model, the cumulative plinth of the H_2O rotational spectrum was subtracted from the model prediction (recall the aforementioned convention in the calculation of the resonance line contribution). Although the general

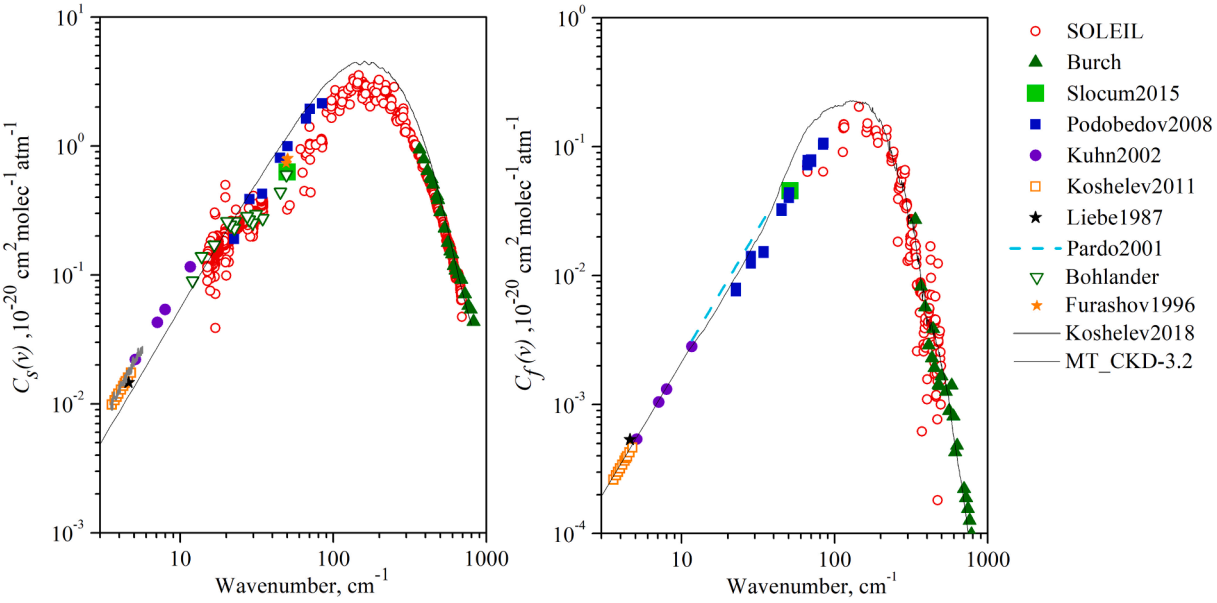

Fig. 1. Self- (left panel) and foreign- (right panel) continuum at 296 K: red circles: SOLEIL measurements [4–7], green triangles: [36,37], blue squares: [35], black star: [41], green empty triangles: measurements of R.A. Bohlander [36], light green square: [45], violet circles: [42], orange empty squares: [40], orange star: [46], grey curve: [47], blue dash curve: [50], black curve: MT_CKD-3.2 model [3]. (For interpretation of the references to colour in this figure legend, the reader is referred to the web version of this article.)

agreement with the MT_CKD-3.2 model is satisfactory (Fig. 1, left panel), the detailed comparison reveals some deviations. The MT_CKD-3.2 model overestimates the self-continuum by about 30% near its maximum. The agreement gradually improves towards the edges of the H_2O band, which is not surprising because experimental results are used for updating the MT_CKD model. However, we note that the model does not reproduce experimental frequency dependence of C_s in the mm and sub-mm wave range (3.5–50 cm^{-1}). In the lower (<10 cm^{-1}) and upper (>20 cm^{-1}) parts of this spectral range, the model systematically underestimates and overestimates the continuum, respectively.

As concerns the foreign-continuum cross-sections determined in the 60–500 cm^{-1} range, they are consistent with the previous experimental studies available in the low- [35,40–42,45,47–50] and high-frequency [36,37] wing of the H_2O band. Again, the MT_CKD-3.2 model shows a very good agreement below 50 cm^{-1} and above 200 cm^{-1}, although some overestimate is notable near the maximum of the band (60–200 cm^{-1}) where previous experimental data were absent.

3. Some insights on the origin of the water continuum

3.1. General outline of atmospheric continuum modeling

The semi-empirical MT_CKD model of the water continuum is the most widely used model for atmospheric applications [51]. It covers the 0 – 20000 cm^{-1} frequency range and is updated periodically as new reliable empirical data on the continuum become available (for instance, Fig. 8 of [52] for the infrared windows). The model is a *far wings model*. The modifying χ-factors of resonance line wings are tuned to ensure agreement with observations, on the assumption that the deviations are due to departures from the Lorentzian profile. The model does not take into account the absorption related to the collisional formation of pair molecular states (although this contribution, in particular, coming from free pairs and partly from metastable dimers, may be partly included in an effective way in the frame of the approach adopted by the model). This may lead to notable differences in the frequency ranges, where the contribution of the dimer absorption is significant. Such deviations were demonstrated in some in-band regions corresponding to fundamental intramolecular vibrational modes of a stable water dimer and their overtones [22,23,53,54]. They are also seen in the range of the pure rotational band of water dimer below 40 cm^{-1} (see Fig. 4 [5] and Fig. 8 [47]).

A general approach to physical modeling of radiation absorption by atmospheric molecules was proposed in [16]. It explicitly takes into account all classes of absorbers that can be collisionally formed in a gas mixture and it does not require the introduction of the uncertain continuum term. We remind below the basic idea of this approach.

The traditionally defined continuum can be expressed in terms of the new approach as will be shown below. The general expression for the total absorption coefficient of a mixture of gases is commonly written as:

$$\alpha(\nu) = \alpha_1(\nu)\rho_1 + \alpha_2(\nu)\rho_2 + \alpha_3(\nu)\rho_3 + \quad (7)$$

where $\alpha_1(\nu)$, $\alpha_2(\nu)$... are the spectra of the corresponding species normalized by their densities ρ_1, ρ_2.... Note that this linear equation is the basis of the traditional approach to the absorption modeling, which neglects the collisional formation of molecular complexes (unaccounted for absorbers) in gases and, therefore, misses the corresponding absorption. The resulting disagreement with observations leads to a need to introduce the continuum. To fix the problem we take into account that monomers of real gas can be in monomolecular, bimolecular, trimolecular *etc*. states. So, a complete exact equation for the total absorption coefficient in real gas (for clarity let us consider pure gas of identical molecules) looks exactly like Eq. (7), but now $\alpha_1(\nu)$ is the spectrum of monomers (in the units of absorption coefficient) normalized by number density of monomers or *monomolecular* absorption, $\alpha_2(\nu)$ is similarly the normalized absorption by molecular pairs or *bimolecular* absorption, $\alpha_3(\nu)$ is similarly trimolecular absorption, and ρ_1, ρ_2... are number densities of the corresponding absorbers. It is obvious that at relatively low pressures, when binary collision approximation is valid, the following relations hold: $\rho_1 = \rho - \rho_2 - \rho_3 - ... \approx \rho$, $\rho_2 = K_2\rho^2$ and $\rho_3 = K_3\rho^3$, where ρ is the total (including those in multimolecular states) number density of monomers, and K_2 and K_3 are the equilibrium constants of bimolecular and trimolecular states. Note that the presence of bimolecular and trimolecular states is taken into account in the virial equation of state of a gas by the second and the third virial coefficients, the values of which are related to the equilibrium constants of bimolecular and trimolecular states [55]. Thus Eq. (7) is written as

$$\alpha(\nu) = \alpha_1(\nu)\rho + \alpha_2(\nu)K_2\rho^2 + \alpha_3(\nu)K_3\rho^3 + \cdots, \quad (8)$$

Note that each contribution (summand of Eq. (8)) may include resonance and non-resonance components. At the same time, the continuum, in accordance with its common definition Eq. (1), includes the total contribution of the second, third and subsequent summands and part of the first summand. Further minor complication of the equation is required for the adequate comparison between various components of absorption of our and traditional approaches. Continuum absorption is usually characterized by the cross-section (absorption coefficient normalized by the product of molecular number density and pressure) in units of $cm^2molec^{-1}atm^{-1}$. These units come from resonance absorption modeling for a variable quantity of absorbing molecules, which involves an integrated line intensity (normalized by molecular number density in $molec/cm^3$) and a collisional line width (normalized by pressure in atm^{-1}). The total absorption (in cm^{-1}) can be written as:

$$\alpha(\nu) = \rho\left[\alpha_1(\nu) + \alpha_2(\nu)K_2\rho k_B T + \alpha_3(\nu)K_3\rho^2(k_B T)^2 + \cdots\right], \quad (9)$$

so α_1 and α_2 are in cm^2molec^{-1}, ρ is in $molec/cm^3$, K_2 and K_3 are in atm^{-1} and atm^{-2}, respectively. Note that the unit of K_2 is $(molec/cm^3)^{-1}$ in Eq. (8), and (atm^{-1}) in Eq. (9). Under atmospheric conditions the components of Eq. (9) starting from the third one are negligible [55]. The bimolecular components of the total absorption (Eq. (9)) can be written as:

$$\begin{aligned} K_2\alpha_2 &= K_{BD}BD + K_{MD}MD + K_F F, \\ K_2 &= K_{BD} + K_{MD} + K_F, \end{aligned} \quad (10)$$

where *BD*, *MD* and *F* (in cm^2molec^{-1}) are the spectra of dimers (stable and metastable) and of free pairs normalized by their density; K_{BD}, K_{MD} and K_F are the equilibrium constants of stable and metastable dimers and free pairs (in atm^{-1}), characterizing their partial pressures (in atm.) as $P_X = K_X P^2 = K_X(\rho kT)^2$, $X = BD, MD, F$. The approach cannot be fully implemented in practical modeling (even within the pair molecular interaction approximation, *i.e.* neglecting the third and all other summands) until sufficient theoretical description is developed for *(i)* bimolecular spectra related to major atmospheric constituents, *i.e.* of H_2O-H_2O, H_2O-N_2, H_2O-O_2, N_2-N_2, N_2-O_2, O_2-O_2, H_2O-Ar, *etc.*, including their free pairs and both stable and metastable dimeric states, and *(ii)* resonance line shape of monomers at large detuning from the line center. In this work, we follow this approach but substitute the missing data by empirical modeling. With these simplifications, we formulate here an alternative to the MT_CKD approach considering both the contributions of bimolecular absorption and far wings of monomer resonance lines. The region of the H_2O rotational band is used for validation tests of the proposed approach.

The dry component of the atmospheric continuum was not considered in the analysis of our SOLEIL spectra because of its negligible amplitude under the used experimental conditions. However, we briefly mention its modeling in the considered spectral range just to demonstrate the relevance of our general approach.

The dry continuum is mainly associated with the pair interactions involving N_2 and O_2 molecules. The monomolecular component of the dry continuum, related to the deviation of the wings of weak resonance lines (quadrupole transitions in N_2 and magnetic-dipole transitions in O_2) from the Lorentzian profile, can be neglected. Note that in some frequency intervals a contribution of both mono- and bimolecular absorptions from other minor atmospheric gas constituents (such as N_2O, CO_2, CH_4, *etc.*) may also become notable [56]. In the range of the H_2O rotational band, the dry continuum is dominated by the roto-translational collision-induced bands of N_2 and O_2 pairs. The bimolecular absorption related to the transient dipole in O_2 induced by collisions with O_2 and N_2 is much weaker than the corresponding absorption in N_2 [9], and thus, the O_2 induced dipole related component can be neglected at least at the current stage of continuum modeling, where the uncertainty of much more important contributions is large. The N_2-N_2 and N_2-O_2 collision induced spectra are quite similar to each-other [9]. Thus, the dry atmospheric continuum spectrum can be roughly modeled in the considered range using the scaling function from [9] and N_2-N_2 continuum spectrum. As included in the HITRAN database [56], the latter is taken from calculations (including the contribution of free pairs, stable and metastable dimers) [57,58], which were recently validated by experiment [10].

As for the wet part of the atmospheric continuum, both self and foreign contributions of bimolecular absorption and the part of monomolecular absorption related to the far wings of water resonance lines are significant. It is necessary to take into account three sets of spectra corresponding to all possible pair states of H_2O-*A* (where *A* is any atmospheric molecule), including truly bound (stable dimer), quasibound (metastable dimer) and free pairs. The H_2O-H_2O, H_2O-N_2 and H_2O-O_2 pair states are expected to bring the dominant contributions. Most of these spectra have never been calculated. However, according to the estimates obtained in [59–64], the concentration of the H_2O-N_2 and H_2O-O_2 heterodimers in air (about 10 ppm near the Earth's surface) is much higher than the concentration of gases, such as CH_4, N_2O, CO and various halocarbons which are of principal importance for the calculation of the greenhouse effect of the Earth's atmosphere. Results of the global rotational-vibrational-tunneling absorption spectrum calculations for H_2O-H_2O stable dimer absorption are available for the 0–600 cm^{-1} region [24]. This allows us to illustrate the application of our approach to the self-continuum. The approach is detailed below and will be applied in the future to the foreign-continuum and thus to the total atmospheric absorption modeling.

3.2. *Some specificities of the self-continuum modeling in the range of H_2O rotational band*

As mentioned above, water vapor self-continuum absorption consists of the absorption by molecular pairs (including stable and metastable dimer states and neglecting minor contribution of free pairs [11–13]) and the absorption related to far wings of water resonance lines.

The stable water dimer contribution (*BD*) in the 0 – 600 cm^{-1} frequency range is discussed on the basis of the *ab initio* calculations of its spectrum [24]. These calculations were validated by a more approximate molecular dynamic approach [65] and by experimental observations of the water dimer rotationally resolved spectrum in the 3.5–8.4 cm^{-1} interval [20,21]. The stable dimer equilibrium constant K_{BD} which is related to its dissociation energy and rules its concentration in water vapor in equilibrium conditions was calculated in [66]. However, the value of K_{BD} retrieved from the rotationally resolved spectrum of the dimer at room temperature [21] turned out to be lower than the calculated value [66] by about 35% (0.036 atm^{-1} at room temperature which corresponds to the 5×10^{-4} relative fraction of stable water dimers in 16 mbar of water vapor). This difference was explained [21] by the fact that the equilibrium constant calculations (Eq. (10) from [66]) involve an overestimated dissociation energy value (1234 cm^{-1}). Indeed, more recent *ab initio* calculations [67] and the velocity map imaging method [68] lead to 1108 cm^{-1} and 1105(10) cm^{-1}, respectively. The equilibrium constant K_{BD} = 0.036 atm^{-1} experimentally retrieved at room temperature corresponds to a dissociation energy of 1144(19) cm^{-1}, which is in a reasonable agreement with the aforementioned values. This K_{BD} value is adopted in the following modeling.

Despite the tremendous progress in *ab initio* calculations of bimolecular spectra [57], the metastable water dimer (metadimer) absorption spectrum has not been calculated yet because of the very high complexity of this system. Following [69], we consider two boundary cases to evaluate the spectrum of the water metadimer. In the first extreme case, a metastable dimer is a double molecule similar to a stable dimer but has a short lifetime. Thus its spectrum is similar to one of stable dimer but homogeneously broadened by the lifetime. Such a model was used in [70,21]. In the second extreme case, a metadimer is considered as two monomers almost freely rotating near each other, and

its absorption spectrum is approximated by the doubled absorption of the monomer also homogeneously broadened due to the short lifetime of the metastable states. This modeling of the metastable dimer spectrum was used in [16,22,70,71]. The unknown lifetime broadening w is a variable parameter of the model which, in principle, depends on the rovibrational transition. Obviously, neither the first nor the second model can reflect all the characteristics of the metadimer spectrum. For example, in the second one, there will be no characteristic features of the rotation of a pair around its center of mass, and in the first one, the characteristic related to the free rotation of monomers is missing. It is supposed [69] that the metadimer spectrum is intermediate between these two boundary cases and thus can be approximated by a linear superposition of the two boundary cases. This approximation is expected to be good in the range of the pure rotational H_2O band because of general similarity of extreme case spectra (both are bell-shaped and their intensity maxima coincide).

The metadimer equilibrium constant, K_{MD}, can be obtained from the well-established (both experimentally and theoretically) value of the second virial coefficient, $B(T)$ [55,72–74]:

$$B(T) = b_0 - K_{BD}RT - K_{MD}RT, \tag{11}$$

where b_0 is an excluded volume, R is a universal gas constant. The excluded volume here represents the part responsible for the free pair states. Empirical approximations of temperature dependences b_0(T) and B(T) can be found in [74,55], respectively.

Keeping in mind the used method of the resonance absorption calculation, the monomolecular component of the total absorption (Eq. (9)) can be written as:

$$\alpha_1 = \alpha_R + W \tag{12}$$

where W is unknown contribution of inadequate resonance line shape modeling at large detuning from the line center. The absorption from the far wings of resonance lines W unaccounted for in α_R is taken into account by a simple model suggested in [16]. It uses (similarly to the MT_CKD model) the empirical χ-function modifying the Lorentzian wings of resonance lines:

$$\chi(\nu - \nu_0) = \left(1 + A\frac{|\nu - \nu_0|}{d\nu_{wing}}\right) exp\left(-\frac{(\nu - \nu_0)^2}{d\nu_{wing}^2}\right), \tag{13}$$

where ν_0 is line center frequency, A and $d\nu_{\text{wing}}$ are the variable parameters corresponding to the intermediate wing amplitude and the characteristic width of the wing, respectively. The model takes into account *(i)* known facts that a real resonance line is "Lorentzian" and "sub-Lorentzian" in the region of near and far wings, respectively [75] and *(ii)* possible "super-Lorentzian" behavior in the range of intermediate wings.

The continuum absorption cross-section $C_S^{calc}(T)$ (in $cm^2molec^{-1}atm^{-1}$) can be thus simulated as a sum of the contributions of stable and metastable dimer absorption and absorption from the far wings of resonance lines:

$$\begin{aligned} C_S^{calc}(T) &= K_{BD}BD(T) + K_{MD}MD(T) + W(T)/P \\ &= K_{BD}D(T) + K_{MD}(kMD_1(T) + (1-k)MD_2(T)) + W(T)/P, \end{aligned} \tag{14}$$

where $MD_1(T)$ and $MD_2(T)$ are the spectra of the metastable dimer according to the first and the second aforementioned extreme cases, respectively, and k is the relative fraction of the first model of the metastable dimer (MD_1) to the total model of the metastable dimer spectrum ($0 \le k \le 1$). To reduce the number of variable parameters, we fix the shape of the stable dimer spectrum to the calculated one (spectrum curves from Fig. 10 from [24]) and the equilibrium constant of the stable water dimer to the value listed in Table 2. The model of the metastable dimer absorption spectrum includes two variable parameters: the fraction parameter, k, and the lifetime, w, assumed to be identical for all the transitions. Its equilibrium constant, K_{MD}, was fixed to the value found from the second virial coefficient, as follows from Eq. (11) (see Table 2). The far-wing contribution is the most uncertain part and includes two parameters (A and $d\nu_{\text{wing}}$) which are adjusted to the measurements.

Table 2
Parameters of the continuum model in the rotational band.

	K_{BD}, atm^{-1} [21]	K_{MD} [a], atm^{-1}	w [b], cm^{-1}	k [c]	A [d]	$d\nu_{wing}$ [e], cm^{-1}
296 K	0.036	0.016	20	1	19	15
326 K	0.017	0.011	30	1	14	15

[a] Constrained to the value derived from Eq. (11).
[b] Lifetime broadening of metastable dimer spectrum MD_2.
[c] Relative fraction of the first model of metastable dimer (MD_1) to the total model of metastable dimer spectrum. Constrained to be identical at 296 K and 326 K.
[d] Intermediate line wing amplitude.
[e] Characteristic width of the super-Lorentzian part of the line wing. Constrained to be identical at 296 K and 326 K.

The temperature dependence of each continuum component is assumed to follow the power law (at least for the relatively narrow T-intervals considered in this work):

$$X(T) = X(T_0)\left(\frac{T_0}{T}\right)^{n_X}, \tag{15}$$

where X refers to BD, MD_1, MD_2 or W, n_X is temperature exponent.

The temperature exponent of the total continuum model is defined as:

$$n = \frac{\ln(C_S^{calc}(T)/C_S^{calc}(T_0))}{\ln(T_0/T)}. \tag{16}$$

3.3. Model validation versus experimental data

The model function of the continuum absorption cross-section $C_S^{calc}(T)$ including its temperature exponent n was optimized to the experimental data available in the range of H_2O rotational band (3.5–600 cm^{-1}), including SOLEIL [4–6] and the literature data [35–37,40–42,45,46]. We used simultaneous ("multispectrum") fitting of the model to continuum cross-sections at 296 K and 326 K and to the continuum temperature exponent n. The final parameters of the model are summarized in Table 2. Note that a change in A and w with temperature is expected, since both the relative speed of molecular movement and the internal energy increase with temperature. The increase in the relative speed of molecular movement leads to the interaction time decrease and, consequently, the decrease of possible non-monotonic interaction, which is responsible for the super-Lorenzian behavior of wings [16]. The increase in the internal energy decreases the average lifetime of metadimers. The contribution of the MD_2 component (like a bound dimer) of the metastable dimer spectrum was found to be negligible. This observation supports the choice of [16,22,70] to model the metadimer spectrum as a broadened monomer spectrum with double intensity in order to analyze the in-band infrared continuum. On the other hand, it may indicate that the experimental K_{BD} value (0.036 atm^{-1} at 296 K) from [21], used in this work, is somewhat overestimated, thus confirming conclusions of the work [76], where the equilibrium constant for true bound dimers (0.016 atm^{-1} at 296 K) was calculated using classical expressions and a complete multidimensional potential energy surface of interacting monomers.

The obtained calculated self-continuum at 296 K and the available experimental data are compared in Fig. 2. The various contributions are presented separately in absolute (left-hand panel) and relative (right-hand panel) scales. An overall good agreement is achieved. Note that the proposed model was constructed in the range up to 600 cm^{-1}, which is

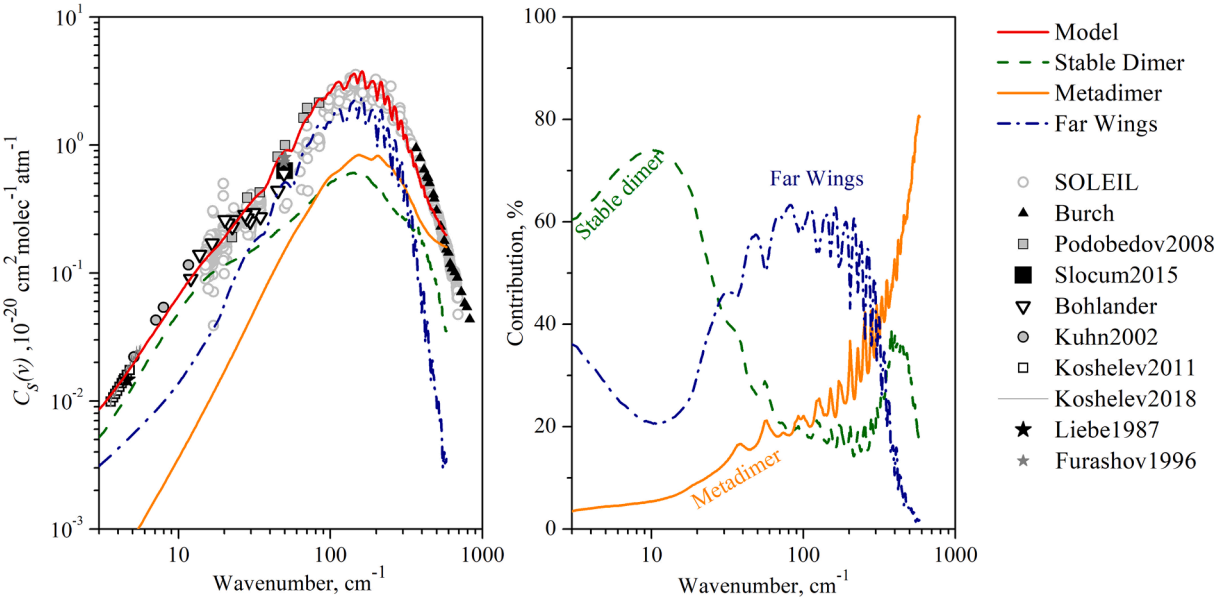

Fig. 2. The self-continuum cross-section (left panel) and relative contribution of continuum components (right panel): grey empty circles: SOLEIL measurements, black triangles: [36,37], grey squares: [35], black star: [41], black empty triangles: measurements by Bohlander [36], black square: [45], black empty squares: [40], grey curve: [47], black circles: [42], grey star: [46], red solid curve: continuum model, green dash curve: stable dimer model, solid curve: metastable dimer model, blue dash-dot curve: far wings model. (For interpretation of the references to colour in this figure legend, the reader is referred to the web version of this article.)

limited by the range of calculated data of the bound dimer spectra [24]. For this reason, the data [36,37] above 600 cm^{-1} were not taken into account in the analysis and are shown in Fig. 2 only for comparison. Compared to our measurements, the largest deviations are observed in the 35 – 84 cm^{-1} interval, where the calculated values are intermediate between our data and those [35]. However, the deviation is within the spread of experimental points.

The temperature exponents – n_{MD1}, n_{MD2} and n_W – of the revealed continuum components at experimental temperatures (296 K and 326 K) can be obtained at this step by substituting their modeled spectra (MD_1, MD_2 and W, respectively) into the following equation:

$$n_X = \frac{\ln(X(T)/X(T_0))}{\ln(T_0/T)}. \quad (17)$$

The temperature exponent of stable dimer absorption, n_{BD}, was estimated by substituting the results of *ab initio* calculations (Fig. 10 from [24]) at 268 K and 308 K into Eq. (17). The temperature exponent of the total continuum in the range of the pure rotational band is calculated from experimental cross-sections using Eq. (16).

The comparison of the experimental and calculated continuum temperature exponents displayed in Fig. 3 shows an agreement within the spread of experimental points (which is quite significant). Note that the temperature exponents n_{BD}, n_{MD1} and n_W are presented separately. The frequency dependence of the temperature exponent in the MT_CKD model is in qualitative agreement with the observations. However, the model overestimates experimental values for frequencies higher than 200 cm^{-1}.

It is worth pointing out that the exclusion of any of the three components from the model significantly worsens the description of the continuum spectrum and its temperature dependence. For example, exclusion of the contribution of a stable dimer leads to significant underestimation of the continuum in the mm-submm range (10–40 cm^{-1}) (see Fig. 2, right-hand panel). On the other hand, dimer absorption (including stable and metastable states) is insufficient to describe the continuum within the entire range of the H_2O pure rotational band. This is especially true around the band intensity maximum. A similar conclusion was made from the analysis of the in-band continuum in the range of fundamental vibrations [16,43]. The exclusion from the model

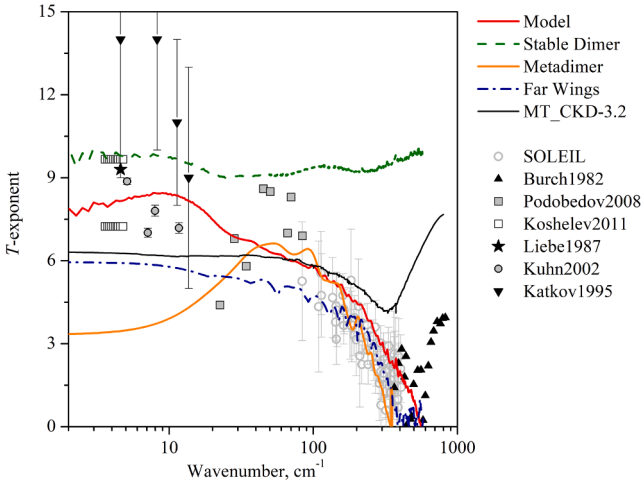

Fig. 3. Self-continuum temperature exponent: grey empty circles: SOLEIL measurements, black triangles: [36,37], grey squares: [35], black star: [41], grey empty squares: [40], black circle: [42], black triangles: [77], red solid curve: continuum model, green dash curve: stable dimer model, orange solid curve: metastable dimer model MD2, blue dash-dot curve: far wings model, black solid curve: MT_CKD-3.2 model [3]. (For interpretation of the references to colour in this figure legend, the reader is referred to the web version of this article.)

of the metadimer contribution leads to an underestimation of the continuum in the high-frequency wing of the rotational band.

3.4. The self-continuum contributors

Detailed consideration of the continuum in the range of wings and center of the band allowed us to draw some conclusions about its contributors. The mm and sub-mm wave ranges (low frequency wing of the H_2O rotational band) are suitable for the detection of stable dimer spectral signature from spectra recorded at temperatures close to atmospheric one. The rotationally resolved water dimer spectrum in close

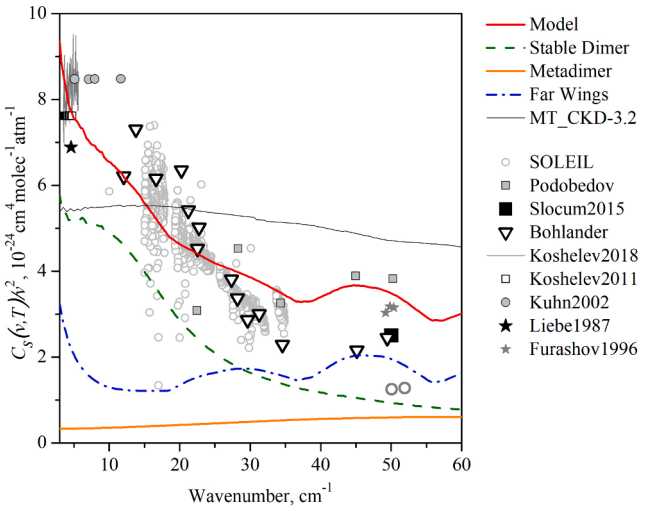

Fig. 4. Continuum spectral function: grey empty circles: SOLEIL measurements [4,5], black empty triangles: [36], grey squares: [35], grey curve: [47], grey empty squares: [40], grey filled circles: [42], grey star: [46], green dash curve: stable dimer model, orange solid curve: metastable dimer model MD_2, blue dash-dot curve: far wings, red solid curve: resulting continuum model, black thin curve: MT_CKD-3.2 model. (For interpretation of the references to colour in this figure legend, the reader is referred to the web version of this article.)

to atmospheric conditions was observed in the 3.5–8.5 cm^{-1} range using the resonator spectrometer [20,21]. The observed sequence of rotational peaks consists of a large number of overlapped lines (*E*-type transitions) corresponding to the end-over-end rotation band of the dimer [78]. The sequence is predicted to reach a broad maximum located at room temperature around 20 cm^{-1}, corresponding to the range of the most intense rotational transitions [24]. This maximum is expected to be located on a wide absorption pedestal smoothly increasing with frequency, due to the other rotation-tunneling transitions of a stable water dimer in the ground and low energy intermolecular vibrational states populated at room temperature. Moreover, a similar smooth frequency dependence of metadimers and absorption related to the far wing of resonance lines is expected because these absorptions reach their maximum at much higher frequencies. In order to separate absorption related to a stable dimer from other sources, the spectral function of the continuum model, $C_S(\nu)/\nu^2$, is considered in this work. The broad absorption maximum due to the dimer rotational absorption near 20 cm^{-1} shows up as a characteristic sharp slope of the spectral function (see Fig. 4). A series of continuum measurements in the sub-THz frequency range (15–35 cm^{-1}) aimed at detecting this spectral signature was performed at SOLEIL [4,5] (see Table 1). The frequency dependence of the measured continuum reproduces the spectral signature of the water dimer predicted by *ab initio* calculations [24]. The available experimental data on the continuum spectral function displayed in Fig. 4 show an overall satisfactory agreement with the model.

In the 15–35 cm^{-1} range, the relative contribution of the stable dimer absorption to the continuum is estimated to be about 50–75%. According to our model, relative contributions of the metadimer absorption and "non-Lorentzian" far wings of resonance water lines are comparable and significantly lower than that of the stable dimer absorption. Note that the increase of the modeled spectral function of far wings in the mm wave range (<5 cm^{-1}) is probably a consequence of the model approximations and should be considered with caution. The analysis of the temperature dependence (Fig. 3) in the mm and sub-mm wave ranges indicates that the temperature exponent of the model (which is within 7–8) is very close to that of a stable water dimer (about 9–10) [6]. This confirms that stable dimers make the dominant contribution in this range.

As illustrated in Fig. 2 (right-hand panel), the contribution of stable dimer absorption to the continuum decreases to 20% in the range of the band intensity maximum (100–300 cm^{-1}), while the metadimer contribution increases with frequency from 20 to 40%. The remaining 40–60% is attributed to the "non-Lorentzian" far wings of resonance water lines. In the high-frequency wing (300–600 cm^{-1}), the metadimer contribution is dominant (40 to 80% of the total absorption), while the stable dimer contributes about 20–35% and the far wings contribution decreases with frequency from 40 to about 2%.

A similar conclusion is follows from the temperature dependence (Fig. 3). The exponent value decreases from 7 to 9 below 50 cm^{-1} to 2 around 300 cm^{-1}. The modeled values of the exponent *n* related to metadimers and non-Lorentzian wings demonstrate a similar behavior, but the calculated values of *n* related to the stable dimers [24] remain high and almost constant. The temperature dependence thus confirms that the relative contribution of the bound dimer decreases with wavenumber, while the contribution of non-Lorentzian wings and metadimers becomes significant.

4. Discussion and conclusions

SOLEIL's experimental data on water vapor continuum reported in [4–7] have been reviewed and analyzed, which allowed us to advance in quantitative characterization and general understanding of the continuum. In particular, the relative contribution of the stable and metastable dimer absorption and far wings of resonance lines has been evaluated in the range of the wings and center of the H_2O rotational band. A physically based modeling of the atmospheric continuum has been proposed and tested with the water self-continuum in the 0–600 cm^{-1} range. The proposed model of the self-continuum, which explicitly takes into account all significant mechanisms, is in a qualitatively good agreement with the observed spectra. The semi-empirical description of non-Lorentzian wings of resonance lines and spectrum of metastable pair states are the major uncertainties of this model. A more accurate description of the wings of resonance lines can be achieved, in our opinion, on the basis of semi-classical trajectory based calculations [58,79]. Currently, this method allows calculating bimolecular absorption by non-polar molecules. The extension of the method to molecules possessing a permanent dipole moment will allow proper calculation of super- and sub-Lorentzian wings of resonance lines. The same approach appears most promising for approximate calculations of the metadimer spectra, until accurate quantum chemical calculations become available. Note that the reproduction of calculations of the bound dimer spectrum either by the trajectory or by the quantum chemical method with the use of an improved potential energy surface of the dimer is also much desired, as well as experimental and theoretical verification of the bound dimer equilibrium constant.

CRediT authorship contribution statement

T.A. Odintsova: Investigation, Formal analysis, Validation, Writing – review & editing. **A.O. Koroleva:** Formal analysis, Validation. **A.A. Simonova:** Formal analysis, Data curation. **A. Campargue:** Conceptualization, Methodology, Writing – review & editing. **M.Yu. Tretyakov:** Conceptualization, Writing – review & editing, Supervision.

Declaration of Competing Interest

The authors declare that they have no known competing financial interests or personal relationships that could have appeared to influence the work reported in this paper.

Acknowledgments

This work becomes possible due to the Project Nos. 20140227, 20180347 and 20170067 supported by Soleil Synchrotron. O. Pirali from SOLEIL is warmly acknowledged for his help during the FTS

recordings. The work was performed under partial financial support from the State Project No. 0030-2021-0016. SA acknowledges support from the Ministry of Science and Higher Education of the Russian Federation (Program of the Basic Scientific Investigations, budget funds for IAO SB RAS, Project No. 121031500297-3).

References

[1] F. Sizov, A. Rogalski, THz detectors, Prog. Quantum Electron. 34 (5) (2010) 278–347.
[2] L. Consolino, S. Bartalini, P. De Natale, Terahertz frequency metrology for spectroscopic applications: a review, J. Infrared Millim. Terahertz Waves. 38 (11) (2017) 1289–1315.
[3] E.J. Mlawer, V.H. Payne, J.L. Moncet, J.S. Delamere, M.J. Alvarado, D.C. Tobin, Development and recent evaluation of the MT CKD model of continuum absorption, Philos. Trans. R. Soc. A Math. Phys. Eng. Sci. 370 (2012) 2520–2556.
[4] T.A. Odintsova, M.Yu. Tretyakov, O. Pirali, P. Roy, Water vapor continuum in the range of rotational spectrum of H_2O molecule: new experimental data and their comparative analysis, J. Quant. Spectrosc. Rad. Transf. 187 (2017) 116–123.
[5] T.A. Odintsova, M.Yu. Tretyakov, A.O. Zibarova, O. Pirali, P. Roy, A. Campargue, Far-infrared self-continuum absorption of $H_2^{16}O$ and $H_2^{18}O$ (15–500 cm^{-1}), J. Quant. Spectrosc. Rad. Transf. 227 (2019) 190–200.
[6] T.A. Odintsova, M.Yu. Tretyakov, A.A. Simonova, I.V. Ptashnik, O. Pirali, A. Campargue, Measurement and temperature dependence of the water vapor self-continuum between 70 and 700 cm^{-1}, J. Mol. Structure. 1210 (2020), 128046.
[7] A.O. Koroleva, T.A. Odintsova, M.Yu. Tretyakov, O. Pirali, A. Campargue, The foreign-continuum absorption of water vapour in the far-infrared (50–500 cm^{-1}), J. Quant. Spectrosc. Rad. Transf. 261 (2021), 107486.
[8] Weakly Interacting Molecular Pairs: Unconventional Absorbers of Radiation in the Atmosphere / ed. by C. Camy-Peyret and A. A. Vigasin. — Dordrecht : Kluwer Academic, 2003. — 287 p. — (NATO ARW Proceedings Series).
[9] J. Boissoles, C. Boulet, R.H. Tipping, A. Brown, Q. Ma, Theoretical calculation of the translation-rotation collision-induced absorption in N_2–N_2, O_2–O_2, and N_2–O_2 pairs, J Quant. Spectr. Radiat. Transf. 82 (1-4) (2003) 505–516.
[10] E.A. Serov, A.A. Balashov, M.Yu. Tretyakov, T.A. Odintsova, M.A. Koshelev, D. N. Chistikov, A.A. Finenko, S.E. Lokshtanov, S.V. Petrov, A.A. Vigasin, Continuum absorption of millimeter waves in nitrogen, J. Quant. Spectrosc. Rad. Transf. 242 (2020), 106774.
[11] A.A. Vigasin, Bound, metastable and free states of bimolecular complexes, Infrared Phys. 32 (1991) 461–470.
[12] C. Leforestier, R.H. Tipping, Q. Ma, Temperature dependences of mechanisms responsible for the water-vapor continuum absorption. II. Dimers and collision-induced absorption, J. Chem. Phys. 132 (2010), 164302.
[13] M.Yu. Tretyakov, A.A. Sisoev, T.A. Odintsova, A.A. Kyuberis, Collision-Induced Dipole Moment and Millimeter and Submillimeter Continuum Absorption in Water Vapor, Radiophys. Quantum Electron. 58 (4) (2015) 262–276.
[14] Q. Ma, R.H. Tipping, C. Leforestier, Temperature dependences of mechanisms responsible for the water-vapor continuum absorption. I. Far wings of allowed lines, J. Chem. Phys. 128 (2008), 124313.
[15] W.M. Elsasser, Mean absorption and equivalent absorption coefficient of a band spectrum, Phys. Rev. 54 (2) (1938) 126–129.
[16] E.A. Serov, T.A. Odintsova, M.Yu. Tretyakov, V.E. Semenov, On the origin of the water vapor continuum absorption within rotational and fundamental vibrational bands, J. Quant. Spectrosc. Rad. Transf. 193 (2017) 1–12.
[17] S.D. Tvorogov, L.I. Nesmelova, O.B. Rodimova, Model description of temperature dependence of the H_2O absorption in 8–14 mm atmospheric window, Atmos. Ocean. Phys. 7 (11–12) (1994) 802–804.
[18] T.E. Klimeshina, O.B. Rodimova, Water-vapor foreign-continuum absorption in the 8–12 and 3–5 μm atmospheric windows, J. Quant. Spectrosc. Rad. Transf. 161 (2015) 145–152.
[19] S. Clough, F. Kneizys, R. Davies, Line shape and water vapor continuum, Atmos. Res. 23 (1989) 229–241.
[20] M.Yu. Tretyakov, E.A. Serov, M.A. Koshelev, V.V. Parshin, A.F. Krupnov, Water dimer rotationally resolved millimeter-wave spectrum observation at room temperature, Phys. Rev. Lett. 110 (2013), 093001.
[21] E.A. Serov, M.A. Koshelev, T.A. Odintsova, V.V. Parshin, M.Yu. Tretyakov, Rotationally resolved water dimer spectra in atmospheric air and pure water vapour in the 188–258 GHz range, Phys. Chem. Chem. Phys. 16 (47) (2014) 26221–26233.
[22] I.V. Ptashnik, K.P. Shine, A.A. Vigasin, Water vapour self-continuum and water dimers: 1. Analysis of recent work, J. Quant. Spectrosc. Rad. Transf. 112 (8) (2011) 1286–1303.
[23] M. Birk, G. Wagner, J. Loos J, K. P. Shine, 3 μm Water vapor self- and foreign-continuum: New method for determination and new insights into the self-continuum, J. Quant. Spectrosc. Rad. Transf. 253 (2020) 107134.
[24] Y. Scribano, C. Leforestier, Contribution of water dimer absorption to the millimeter and far infrared atmospheric water continuum, J. Chem. Phys. 126 (2007), 234301.
[25] H.G. Kjaergaard, A.L. Garden, G.M. Chaban, R.B. Gerber, D.A. Matthews, J. F. Stanton, Calculation of vibrational transition frequencies and intensities in water dimer: comparison of different vibrational approaches, J. Phys. Chem. A 112 (18) (2008) 4324–4335.
[26] T. Salmi, V. Hänninen, A.L. Garden, H.G. Kjaergaard, J. Tennyson, L. Halonen, Calculation of the O-H stretching vibrational overtone ssptrum of the water dimer, J. Phys. Chem. A. 112 (28) (2008) 6305–6312.
[27] I.E. Gordon, L.S. Rothman, C. Hill, R.V. Kochanov, Y. Tan, P.F. Bernath, M. Birk, V. Boudon, A. Campargue, K.V. Chance, B.J. Drouin, J.-M. Flaud, R.R. Gamache, J. T. Hodges, D. Jacquemart, V.I. Perevalov, A. Perrin, K.P. Shine, M.-A.-H. Smith, J. Tennyson, G.C. Toon, H. Tran, V.G. Tyuterev, A. Barbe, A.G. Császár, V.M. Devi, T. Furtenbacher, J.J. Harrison, J.-M. Hartmann, A. Jolly, T.J. Johnson, T. Karman, I. Kleiner, A.A. Kyuberis, J. Loos, O.M. Lyulin, S.T. Massie, S.N. Mikhailenko, N. Moazzen-Ahmadi, H.S.P. Müller, O.V. Naumenko, A.V. Nikitin, O.L. Polyansky, M. Rey, M. Rotger, S.W. Sharpe, K. Sung, E. Starikova, S.A. Tashkun, J.V. Auwera, G. Wagner, J. Wilzewski, P. Wcisło, S. Yu, E.J. Zak, The HITRAN2016 molecular spectroscopic database, J. Quant. Spectrosc. Rad. Transf. 203 (2017) 3–69.
[28] J.H. Van Wleck, D.L. Huber, Absorption, emission, and linebreadths: A semihistorical perspective, Rev. Mod. Phys. 49 (4) (1977) 939–959.
[29] G.Yu. Golubiatnikov, V.N. Markov, A. Guarnieri, R. Knöchel, Hyperfine Structure of $H_2^{16}O$ and $H_2^{18}O$ measured by Lamb-dip technique in the 180–560 GHz frequency range, J. Mol. Spectrosc. 240 (2) (2006) 251–254.
[30] G.Yu. Golubiatnikov, Shifting and broadening parameters of the water vapor 183-GHz line (3_{13}–2_{20}) by H_2O, O_2, N_2, CO_2, H_2, He, Ne, Ar, and Kr at room temperature, J. Mol. Spectrosc. 230 (2) (2005) 196–198.
[31] G.Yu. Golubiatnikov, M.A. Koshelev, A.F. Krupnov, Pressure shift and broadening of 1_{10}–1_{01} water vapor lines by atmosphere gases, J. Quant. Spectrosc. Radiat. Transf. 109 (2008) 1828–1833.
[32] M.A. Koshelev, Collisional broadening and shifting of the 2_{11}–2_{02} transition of $H_2^{16}O$, $H_2^{17}O$, $H_2^{18}O$ by atmosphere gases, J. Quant. Spectrosc. Radiat. Transf. 112 (2011) 550–552.
[33] M.A. Koshelev, M.Yu. Tretyakov, G.Yu. Golubiatnikov, V.V. Parshin, V.N. Markov, I.A. Koval, Broadening and shifting of the 321-, 325- and 380-GHz lines of water vapor by the pressure of atmospheric gases, J. Mol. Spectrosc. 241 (2007) 101–108.
[34] M.Yu. Tretyakov, M.A. Koshelev, I.N. Vilkov, V.V. Parshin, E.A. Serov, Resonator Spectroscopy of the Atmosphere in the 350–500 GHz Range, J. Quant. Spectrosc. Radiat. Transf. 114 (2013) 109–121.
[35] V.B. Podobedov, D.F. Plusquellic, K.E. Siegrist, G.T. Fraser, Q. Ma, R.H. Tipping, New measurements of the water vapor continuum in the region from 0.3 to 2.7 THz, J. Quant. Spectrosc. Radiat. Transf. 109 (3) (2008) 458–467.
[36] D. Burch, Continuum absorption by atmospheric H_2O, Proc. SPIE. 277 (1981) 28–39.
[37] D.E. Burch, R.L. Alt, Continuum absorption by H_2O in the 700-1200 cm^{-1} and 2400-2800 cm^{-1} windows, US Air Force Geophysics Laboratory report AFGL-TR-84–0128, Hanscom Air Force Base, MA, USA(1984).
[38] A. Campargue, S. Kassi, D. Mondelain, S.S. Vasilchenko, D. Romanini, Accurate laboratory determination of the near infrared water vapor self-continuum. A test of the MT_CKD model, J. Geophys. Res. Atmos. 121 (21) (2016) 13180–13203.
[39] A. Bauer, M. Godon, J. Carlier, R.R. Gamache, Continuum in the windows of the water vapor spectrum absorption of H_2O-Ar at 239 GHz and linewidth calculations, J. Quant. Spectrosc. Radiat. Transfer. 59 (3–5) (1998) 273–285.
[40] M.A. Koshelev, E.A. Serov, V.V. Parshin, M.Yu. Tretyakov, Millimeter wave continuum absorption in moist nitrogen at temperatures 261–328 K, J. Quant. Spectr. Radiat. Transf. 112 (2011) 2704–2712.
[41] H.J. Liebe, D.H. Layton, Millimeter-wave properties of the atmosphere: Laboratory studies and propagation modeling, NTIA Rep. (1987) 87–224.
[42] T. Kuhn, A. Bauer, M. Godon, S. Buehler, K. Kuenzi, Water vapor continuum: absorption measurements at 350 GHzand model calculations, J. Quant. Spectrosc. Radiat. Transf. 74 (2002) 545–562.
[43] I.V. Ptashnik, T.E. Klimeshina, A.A. Solodov, A.A. Vigasin, Spectral composition of the water vapour self-continuum absorption within 2.7 and 6.25 μm bands, J. Quant. Spectrosc. Radiat. Transf. 228 (2019) 97–105.
[44] A.A. Vigasin, Water vapor continuous absorption in various mixtures: possible role of weakly bound complexes, J. Quant. Spectrosc. Radiat. Transf. 64 (1) (2000) 25–40.
[45] D. Slocum, R. Giles, T. Goyette, High-resolution water vapor spectrum and line shape analysis in the Terahertz region, J. Quant. Spectrosc. Radiat. Transf. 159 (2015) 69–79.
[46] N.I. Furashov, B.A. Sverdlov, S.N. Chernyaev, Absorption of electromagnetic radiation by pure water vapor at frequencies near 1.5 THz, Radiophysics and Quantum electronics 39 (9) (1996) 754–759.
[47] M.A. Koshelev, I.I. Leonov, E.A. Serov, A.I. Chernova, A.A. Balashov, G.M. Bubnov, A.F. Andriyanov, A.P. Shkaev, V.V. Parshin, A.F. Krupnov, M.Yu. Tretyakov, New frontiers of modern resonator spectroscopy, IEEE Trans. Terahertz Sci. Technol. 8 (6) (2018) 773–783.
[48] J.-G. Kwon, M.-W. Park, T.-I. Jeon, Determination of the water vapor continuum absorption by THz pulse transmission using long-range multipass cell, J. Quant. Spectrosc. Radiat. Transf. 272 (2021), 107811.
[49] Y. Yang, M. Mandehgar, D. Grischkowsky, Determination of the water vapor continuum absorption by THz-TDS and Molecular Response Theory, Opt. Express. 22 (4) (2014) 4403.
[50] J.R. Pardo, E. Serabyn, J. Cernicharo, Submillimeter atmospheric transmission measurements on Mauna Kea during extremely dry El Nino conditions: implications for broadband opacity contributions, J. Quant. Spectrosc. Rad. Transf. 68 (2001) 419–433.
[51] M.J. Alvarado, V.H. Payne, E.J. Mlawer, G. Uymin, M.W. Shephard, K.E. Cady-Pereira, J.S. Delamere, J.-L. Moncet, Performance of the Line-By-Line Radiative Transfer Model (LBLRTM) for temperature, water vapor, and trace gas retrievals:

recent updates evaluated with IASI case studies, Atmos. Chem. Phys. 13 (2013) 6687–6711.
[52] L. Lechevallier, S. Vasilchenko, R. Grilli, D. Mondelain, D. Romanini, A. Campargue, The water vapour self-continuum absorption in the infrared atmospheric windows: new laser measurements near 3.3 and 2.0 μm, Atmos. Meas. Tech. 11 (2018) 2159–2171.
[53] Yu.I. Baranov, W.J. Lafferty, The water-vapor continuum and selective absorption in the 3 to 5 μm spectral region at temperatures from 311 K to 363 K, Quant. Spectrosc. Rad. Transf. 112 (2011) 1304–1313.
[54] A.A. Simonova, I.V. Ptashnik, J. Elsey, R.A. McPheat, K.P. Shine, K.M. Smith, Water vapour self-continuum in near-visible IR absorption bands: Measurements and semiempirical model of water dimer absorption, J. Quant. Spectrosc. Rad. Transf. 277 (2022) 107957.
[55] M.Yu. Tretyakov, E.A. Serov, T.A. Odintsova, Equilibrium thermodynamic state of water vapor and the collisional interaction of molecules, Radiophys. Quantum Electron. 54 (10) (2012) 700–716.
[56] T. Karman, I.E. Gordon, A.d. van der Avoird, Y.I. Baranov, C. Boulet, B.J. Drouin, G.C. Groenenboom, M. Gustafsson, J.-M. Hartmann, R.L. Kurucz, L.S. Rothman, K. Sun, K. Sung, R. Thalman, H.a. Tran, E.H. Wishnow, R. Wordsworth, A. A. Vigasin, R. Volkamer, W.J. van der Zande, Update of the HITRAN collision-induced absorption section, Icarus 328 (2019) 160–175.
[57] T. Karman, E. Miliordos, K.L.C. Hunt, G.C. Groenenboom, A. van der Avoird, Quantum mechanical calculation of the collision-induced absorption spectra of N_2–N_2 with anisotropic interactions, J. Chem. Phys. 142 (2015), 084306.
[58] D.N. Chistikov, A.A. Finenko, S.E. Lokshtanov, S.V. Petrov, A.A. Vigasin, Simulation of collision-induced absorption spectra based on classical trajectories and ab initio potential and induced dipole surfaces. I. Case study of N_2–N_2 rototranslational band, J. Chem. Phys. 151 (19) (2019) 194106.
[59] I.M. Svishchev, R.J. Boyd, Van der Waals complexes of water with oxygen and nitrogen: infrared spectra and atmospheric implications, J. Phys. Chem. A. 102 (37) (1998) 7294–7296.
[60] V. Vaida, J.E. Headrick, Physicochemical Properties of Hydrated Complexes in the Earth's Atmosphere, J. Phys. Chem. A. 104 (23) (2000) 5401–5412.
[61] T.W. Robinson, H.G. Kjaergaard, High level *ab initio* studies of the low-lying excited states in the H_2O–O_2 complex, J. Chem. Phys. 119 (7) (2003) 3717–3720.
[62] H.G. Kjaergaard, T.W. Robinson, D.L. Howard, J.S. Daniel, J.E. Headrick, V. Vaida, Complexes of importance to the absorption of solar radiation, J. Phys. Chem. A. 107 (49) (2003) 10680–10686.
[63] A. Sabu, S. Kondo, R. Saito, Y. Kasai, K. Hashimoto, Theoretical study of O_2–H_2O: Potential energy surface, molecular vibrations, and equilibrium constant at atmospheric temperatures, J. Phys. Chem. A. 109 (2005) 1836–1842.
[64] Yu.I. Baranov, I.A. Buryak, S.E. Lokshtanov, V.A. Lukyanchenko, A.A. Vigasin, H_2O-N_2 collision-induced absorption band intensity in the region of the N_2 fundamental: *ab initio* investigation of its temperature dependence and comparison with laboratory data, Phil. Trans. R. Soc. A. 370 (2012) 2691–2709.
[65] M.-S. Lee, F. Baletto, D.G. Kanhere, S. Scandolo, Far-infrared absorption of water clusters by first-principles molecular dynamics, J. Chem. Phys. 128 (2008), 214506.
[66] Y. Scribano, N. Goldman, R.J. Saykally, C. Leforestier, Water Dimers in the Atmosphere III: Equilibrium Constant from a Flexible Potential, J. Phys. Chem. A. 110 (2006) 5411–5419.
[67] C. Leforestier, K. Szalewicz, A. van der Avoird, Spectra of water dimer from a new ab initio potential with flexible monomers, J. Chem. Phys. 137 (2012), 014305.
[68] B.E. Rocher-Casterline, A.K. Mollner, L.C. Ch'ng, H. Reisler, Imaging H2O photofragments in the predissociation of the HCl-H_2O hydrogen-bonded dimer, J. Phys. Chem. A. 115 (25) (2011) 6903–6909.
[69] A.A. Vigasin, On the possibility to quantify contributions from true bound and metastable pairs to infrared absorption in pressurised water vapour, Mol. Phys. 108 (18) (2010) 2309–2313.
[70] T.A. Odintsova, M.Yu. Tretyakov, Evidence of true bound and metastable dimers and trimers presence in high temperature water vapor spectra, J. Quant. Spectrosc. Rad. Transf. 120 (2013) 134–137.
[71] A.A. Simonova, I.V. Ptashnik, Water vapor self-continuum model in the rotational absorption band, Proc. SPIE. 1156002 (2020) 1–7.
[72] D.E. Stogryn, J.O. Hirschfelder, Contribution of bound, metastable, and free molecules to the second virial coefficient and some properties of double molecules, J. Chem. Phys. 31 (6) (1959) 1531–1545.
[73] W. Wagner, A. Pruß, The IAPWS formulation 1995 for the thermodynamic properties of ordinary water substance for general and scientific use, J. Phys. Chem. Ref. Data 31 (2) (2002) 387–535.
[74] C. Leforestier, Water dimer equilibrium constant calculation: A quantum formulation including metastable states, J. Chem. Phys. 140 (2014), 074106.
[75] S.A. Clough, F.X. Kneizys, R. Davies, R. Gamache, R. Tipping, Theoretical lineshape for H_2O vapor; application to the continuum, in: A. Deepak, T.D. Wilkerson, L. H. Ruhnke (Eds.), Atmospheric water vapor, Academic Press, New York, 1980, p. 25.
[76] I. Buryak, A.A. Vigasin, Classical calculation of the equilibrium constants for true bound dimers using complete potential energy surface, J. Chem. Phys. 143 (2015), 234304.
[77] V.Yu. Katkov, B.A. Sverdlov, N.I. Furashov, Experimental estimates of the value and temperature dependence of the air-humidity quadratic component of the atmospheric water-vapor absorption coefficient in the frequency band of 140–410 GHz, Radiophys. Quantum Electron. 38 (12) (1995) 835–844.
[78] A.F. Krupnov, M.Yu. Tretyakov, C. Leforestier, Possibilities of the observation of the discrete spectrum of the water dimer at equilibrium in millimeter-wave band, J. Quant. Spectrosc. Rad. Trans. 110 (8) (2009) 427–434.
[79] D.N. Chistikov, A.A. Finenko, Yu. N. Kalugina, S.E. Lokshtanov, S.V. Petrov, A. A. Vigasin, Simulation of collision-induced absorption spectra based on classical trajectories and ab initio potential and induced dipole surfaces. II. CO_2–Ar rototranslational band including true dimer contribution, J. Chem. Phys. 155 (6) (2021), 064301.